N95- 13963

THE PHOTON: EXPERIMENTAL EMPHASIS ON ITS WAVE-PARTICLE DUALITY

Y. H. Shih, A. V. Sergienko and M. H. Rubin
Department of Physics, University of Maryland
Baltimore County, Baltimore, MD 21228

T. E. Kiess, C. O. Alley
Department of Physics, University of Maryland,
College Park, MD 20742

Abstract

Two types of Einstein-Podolsky-Rosen experiments were demonstrated recently in our laboratory. It is interesting to see that in an interference experiment (wave-like experiment) the photon exhibits its particle property, and in a beam-splitting experiment (particle-like experiment) the photon exhibits its wave property. The two-photon states are produced from Type I and Type II optical spontaneous parametric down conversion, respectively.

We wish to report two EPR [1] type experiments. The first one is a two-photon interference experiment in a standard Mach-Zehnder interferometer. Another one is a two-photon beam-splitting type experiment for the measurement of polarization correlation. It is interesting to see that in the interference experiment (wave-like experiment) the photon exhibits its particle property, and in the beam-splitting experiment (particle-like experiment) the photon exhibits its wave property.

I Two-photon interference in a standard Mach-Zehnder interferometer.

A pair of photons with different colors ($\lambda_1 = 632.8\ nm, \lambda_2 = 788.7\ nm, 155.9nm$ difference in center wavelength) is directed to one input port of a Mach-Zehnder interferometer. Coincidence

measurement is made between the two output ports of the interferometer with the help of a 300 psec coincidence time window. The interference behavior was studied in a wide range of the optical path difference of the interferometer from white light condition, $\Delta L \cong 0$, to about $\Delta L \cong 127cm$ ($\cong 2 \cdot 10^3$ times the coherence length of the down converted beams). When the optical delay of the interferometer is greater than the coincidence time window, the amplitudes in which one photon follows the longer arm and the other follows the shorter arm of the interferometer are "cut off" by the coincidence time window. The particle property of the photon is demonstrated by means of more than 50% interference visibility.

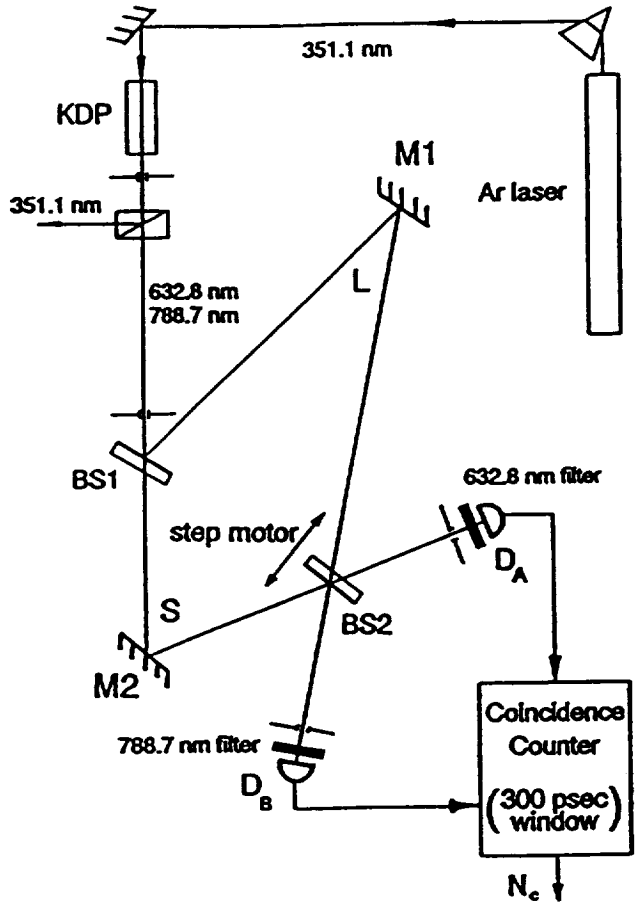

Figure I-1: Schematic diagram of the experiment.

The experimental arrangement is shown in fig. I-1. A $10cm$ long Type I phase matching KDP crystal pumped by a single mode $351.1nm$ CW Argon ion laser line is used to generate collinear photon pairs at wavelengths $632.8nm$ and $788.7nm$. The coherence length of the pump beam was measured to be longer than $5m$. The $351.1nm$ pump beam and the down converted beams were polarized in the extraordinary and ordinary ray directions of the crystal, respectively. A Glan-Thompson prism was used to separate the collinear down converted photon beams from the orthogonal polarized $351.1nm$ pump beam. Before the $351.1nm$ laser line was sent to pump the parametric down conversion, a quartz dispersion prism was used to separate out the radiation

lines of the laser plasma tube which are close to the $632.8nm$ and $788.7nm$ wavelengths.

The collinear $632.8nm$ and $788.7nm$ photon pair was then injected into a standard Mach-Zehnder interferometer. The optical path differences of the interferometer $\Delta L = L - S$ can be arranged to be shorter or longer than the coherence length, l_{coh}, of each beam of the down conversion field and the coincidence time window, $c \cdot \Delta T_{coin}$. The collinear photon pairs were injected onto the beamsplitter with an incident angle of about ten to twelve degrees (near normal), for which the reflected and transmitted intensities of the $632.8nm$ and $788.7nm$ beams were measured to be equal $(50\% - 50\%)$ within 5%.

Geiger mode avalanche photodiode detectors, operated at dry ice temperature, were used to record coincidences in the two output ports of the Mach-Zehnder interferometer. Each of the detector has a narrow band interference spectral filters. The central wavelengths of the filters are $632.8nm$ and $788.8nm$ with bandwidths of $1.4nm$ and $1.7nm$, respectively. The output pulses from detector A and detector B were then sent to N_1, N_2 counter and a coincidence circuit to record coincidences. The coincidence time window ΔT_{coin} was about $300psec$.

We collected data for three regions of interest. In the first region, $\Delta L < l_{coh}$, i.e., the optical paths difference of the interferometer are equal to within the first order coherence length of the signal and idler. In the second region, $l_{coh} < \Delta L < c \cdot \Delta T_{coin}$. In the third region, $\Delta L > c \cdot \Delta T_{coin}$. The following reported data are all direct measured values without any noise reductions or theoretical corrections.

(1). The first region, $\Delta L < l_{coh}$.

Fig. I-2 shows the normalized counting rate of N_c when the optical path difference changed from white light condition to about $4\mu m$. In this region, N_1 and N_2 both showed clear single wavelength, $632.8nm$ and $788.7nm$, respectively, first order interference pattern. However, N_c shows a complecated interference pattern with $632.8nm, 788.7nm$, and the beating and the sum frequencies. The interference visibility is close to 100% with the $300psec$ coincidence window. The solid curve in fig. I-2 is a theoretical fitting of equation (I-10). Fig. I-3 shows a typical first order interference pattern of N_2 for detector B. The interference visibility is about 90%, with a period corresponding to wavelength $788.7nm$.

Fig. I-4 shows the typical interference patterns of N_c at $\Delta L \cong 115\mu m$. The N_c pattern in fig. I-4 is different than that in fig. I-2 in two ways, (A) the interference visibility is reduced and, (B) the beating component and the $632.8nm$ and $788.7nm$ components of the modulations are reduced and the sum-frequency modulation becomes predominant. The solid line in fig. I-4 is a theoretical curve resulting from Gaussian spectral filter functions in equation (I-10). The single detector counting rate is reported in fig. I-5. The interference visibility is reduced to about 42%.

(2). The second region, $l_{coh} < \Delta L < c \cdot \Delta T_{coin}$.

In this region both N_1 and N_2 become constant, however, N_c shows clear interference with the sum frequency. Fig. I-6 shows the interference pattern of N_c for $\Delta L \cong 0.5cm$. Compare to the 300 psec coincidence time window and the coherent length of the down converted beams, which satisfying $l_{coh} < \Delta L < c \cdot \Delta T_{coin}$. The interference visibility is $44\% \pm 3\%$ with modulation at a wavelength of $351.1nm$. In this region, all the measured interference patterns have modulation visibilities close to but less then 50%.

(3). The third region,$\Delta L > c \cdot \Delta T_{coin}$.

The interference patterns of N_c in the final region of interest, $\Delta L > c \cdot \Delta T_{coin}$, is presented in fig. I-7. An interference visibility of $75\% \pm 3\%$ was measured at $\Delta L \cong 43cm$ with an interference

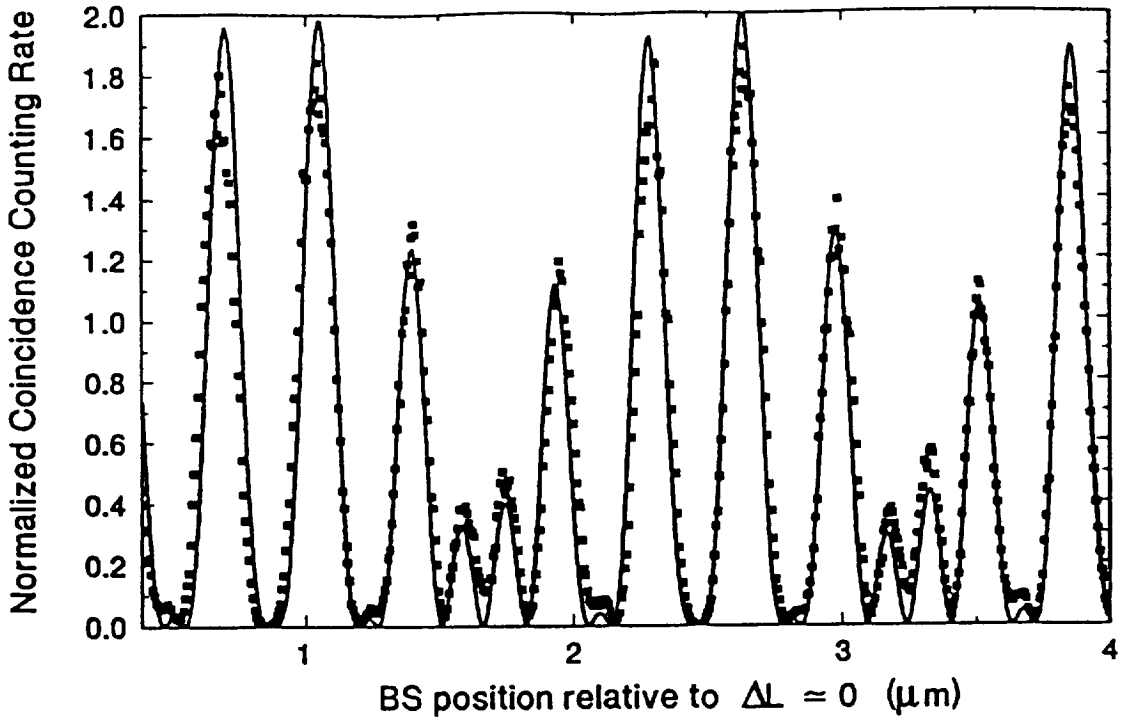

Figure I-2: Normalized coincidence counting rate of $N_c$at near white light condition ($\Delta L \cong 0$). The beting frequency,with 3.2μmperiod, and sum frequency, with 351.1nmperiod, are evident from the graph. Signal and idler frequencies, at periods 632.8nm and 788.7nm also contribute. The solid line is a theoretical curve of Eq. (I-10).

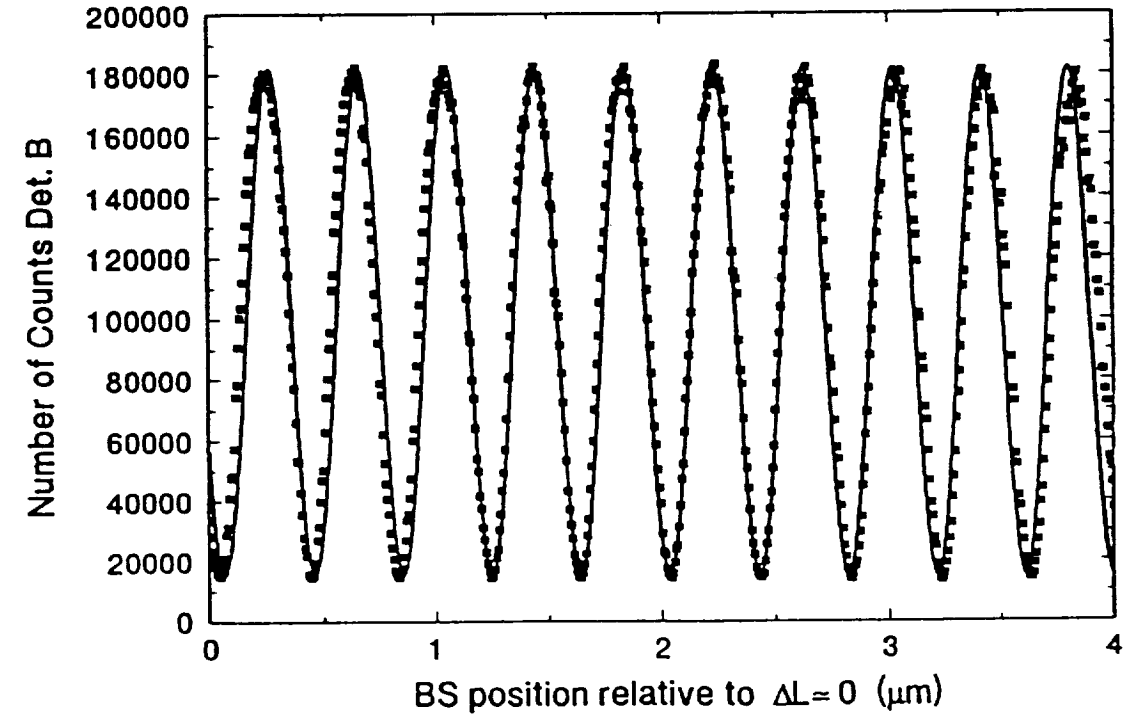

Figure I-3: Single detector counting rate N_2 at near white light condition ($\Delta L \cong 0$).

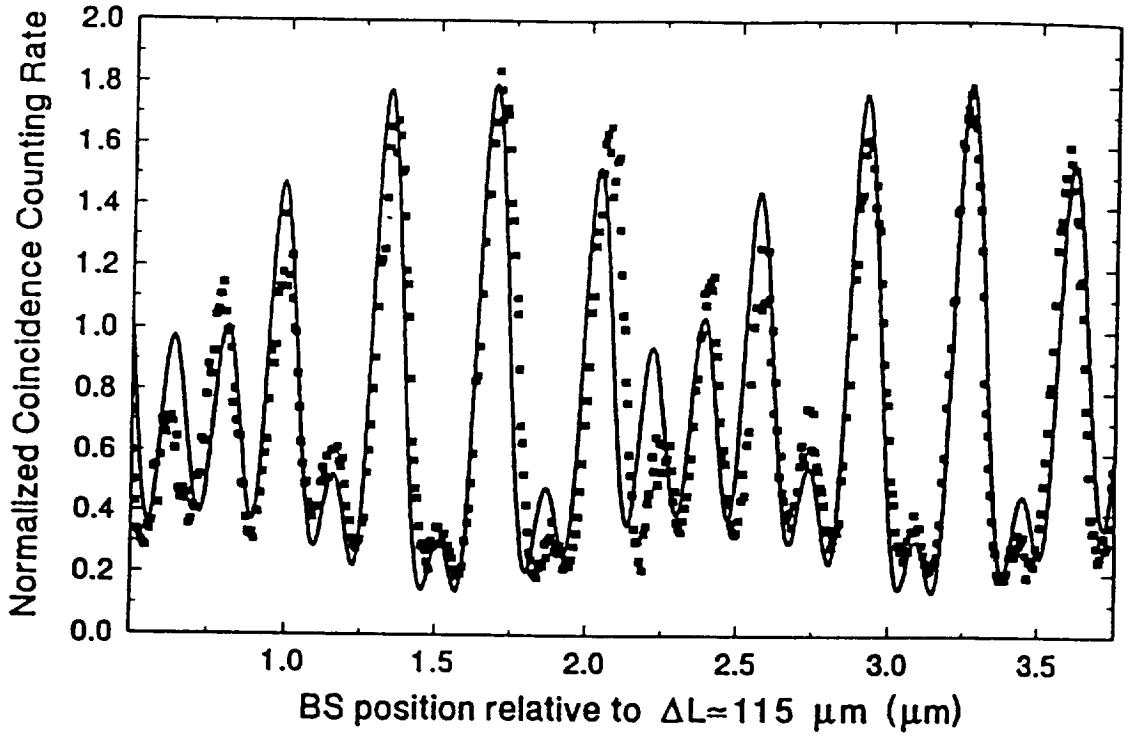

Figure I-4: Normalized coincidence counting rate of N_c at $\Delta L \cong 115\ \mu m$. Compared with fig. I-2, the beating component and the ω_1 and ω_2 components of the modulation are reduced and the sum-frequency modulation becomes predominant. The solid line is a theoretical curve resulting from Gaussian spectral distributions in Eq. (I-10).

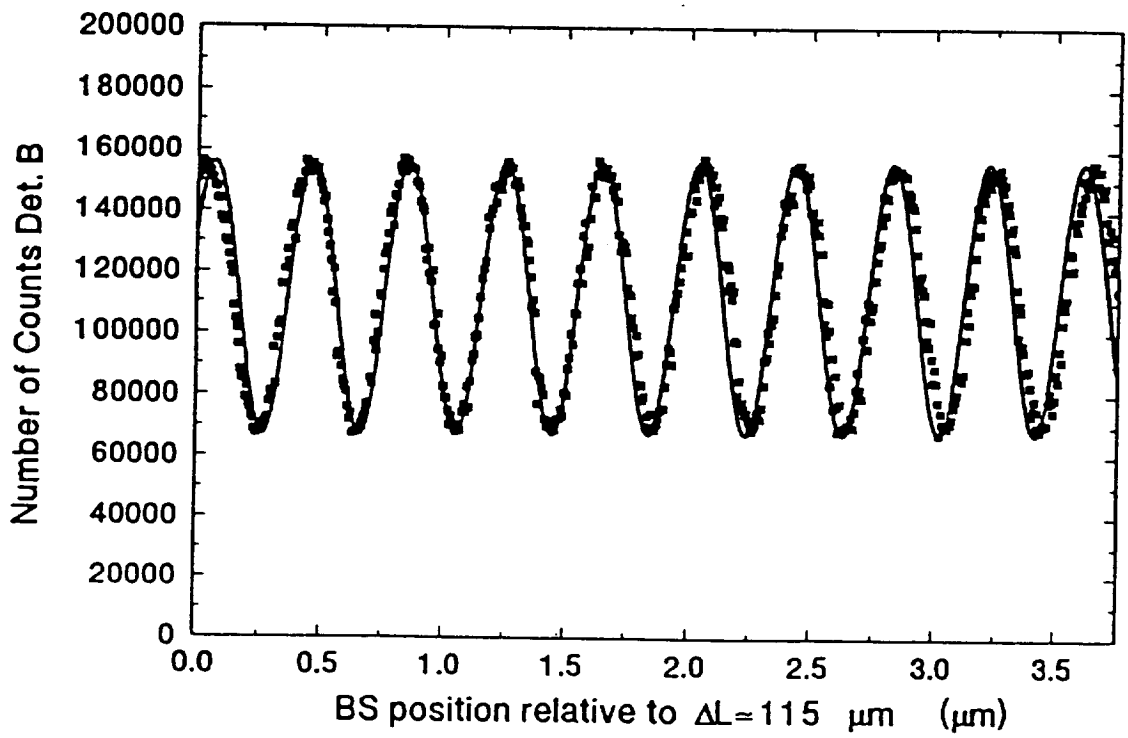

Figure I-5: Single detector counting rate N_2 at $\Delta L \cong 115\ \mu m$.

period of $351.1nm$. When ΔL increased to about $127cm$, the interference visibility was measured to be $56\% \pm 3\%$. In this region, no interference modulations were found for N_1 and N_2.

In our earlier paper [2] a general theory for a two photon interference experiment in two interferometers was developed. The experiment was suggested by Franson [3]. Experimental study for two independent interferometers have demonstrated more than 50% interference visibility by using short time coincidence time windows [4, 5]. The theory for this experiment is similar. The coincidence counting rate is calculated from the field fourth order correlation function:

$$G(r_1t_2, r_2t_2; r_2t_2, r_1t_1) =< E_1^{(-)}E_2^{(-)}E_2^{(+)}E_1^{(+)} > \qquad (\mathrm{I}-1)$$

where $E_j^{(+)}$ is the positive frequency part of the electric field in the Heisenberg picture evaluated at the position r_j and the time t_j. $E_j^{(-)}$ is the hermitian conjugate of $E_j^{(+)}$,

$$E_j^{(+)}(t_j) = \int d\omega f_j(\omega)e^{-i\omega t}a_j(\omega) \qquad (\mathrm{I}-2)$$

a_j is the destruction operator of the photons in the jth beam and f_j is the pass band of the filter in the beam peaked at Ω_j. We take $\Omega_1 + \Omega_2 = \omega_p$, the pump frequency. In this experiment the filters are chosen so that each detector only detects one of the down converted beam, i.e., $\Omega_1 - \Omega_2 >> \sigma$ the band width of the filters.

The average coincidence counting rate is given by

$$\begin{aligned} R_c &= \tfrac{1}{T}\iint_0^T dt_1dt_2G(r_1t_1, r_2t_2, r_2t_2, r_1t_1)S(t_1 - t_2, \Delta T_{coin}) \\ &= \tfrac{1}{T}\iint_0^T dt_1dt_2 \mid \langle 0 \mid E_1^{(+)}(t_1), E_2^{(+)}(t_2) \mid \Psi\rangle \mid^2 S(t_1 - t_2, \Delta T_{coin}) \end{aligned} \qquad (\mathrm{I}-3)$$

where $S(t, \Delta T_{coin})$ is a coincidence detection function, ΔT_{coin} is the coincidence time window, and the integrals are over the detection time T. A two photon amplitude, which is also called effective two-photon wavefunction, is defined in (I-3) by,

$$\Psi(t_1, t_2) =< 0 \mid E_1^{(+)}(t_1)E_2^{(+)}(t_2) \mid \Psi > \qquad (\mathrm{I}-4)$$

The two photon part of the state that emerging from the down conversion crystal may be taken to be [6],

$$\mid \Psi >= \iint d\omega_1 d\omega_2 \delta(\omega_1 + \omega_2 - \omega_p)a_1^\dagger(\omega_1)a_2^\dagger(\omega_2) \mid 0 > \qquad (\mathrm{I}-5)$$

where the δ function indicate a perfect frequency phase matching condition. The wave number phase matching condition is implicit in the choice of the location of the pinholes and the detectors. Substitute (I-4) and (I-5) into (I-3), it is straight forward to show that,

$$\Psi(t_1, t_2) = A(t_1, t_2) + A(t_1 - \Delta T, t_2 - \Delta T) + A(t_1, t_2 - \Delta T) + A(t_1 - \Delta T, t_2) \qquad (\mathrm{I}-6)$$

where $A(t_1, t_2)$ is calculated in (I-8), $\Delta L = c \cdot \Delta T$ is the optical path difference in the two arms of the interferometer. The first (second) term is the amplitude for which both photons follow the short (long) path through the interferometer, and the third (fourth) term is the amplitude for one photon follows the short (long) path and another photon follows the long (short) path. A simple calculation using Gaussian filters

$$f_j = \exp[-(\omega - \Omega_j)^2/2\sigma_j^2] \qquad (\mathrm{I}-7)$$

where σ_j is the bandwidth of the jth filter, gives

$$A(t_1,t_2) = \exp[-i(\Omega_1 t_1 + \Omega_2 t_2)]u(t_1 - t_2)$$
$$u(t) = K\exp[-\Sigma^2 t^2/2]; 1/\Sigma^2 = 1/\sigma_1^2 + 1/\sigma_2^2 \qquad (I-8)$$

where K is a constant.

If we now substitute equations (I-6) and (I-7) into (I-3) and take

$$S(t,\Delta T_{coin}) = \exp(-\mid t \mid /2\Delta T_{coin}) \qquad (I-9)$$

the average counting rate may be written in the form

$$R_c = R_0[J_0 + J_1\cos(\Omega_1\Delta T) + J_1\cos(\Omega_2\Delta T) +$$
$$J_+\cos(\Omega_1\Delta T - \Omega_2\Delta T) + J_-\cos(\Omega_1\Delta T + \Omega_2\Delta T) \qquad (I-10)$$

where

$$J_0 = C[2erfc(\Lambda) + \exp(-\Delta T/2\Delta T_{coin})erfc(\Lambda + \Sigma\Delta T/2)$$
$$+\exp(-\Delta T/2\Delta T_{coin})erfc(\Lambda - \Sigma\Delta T/2)$$
$$J_1 = 2C\exp(-\Sigma^2\Delta T^2/4)[\exp(-\Delta T/4\Delta T_{coin})erfc(\Lambda + \Sigma\Delta T/2)$$
$$+\exp(-\Delta T/4\Delta T_{coin})erfc(\Lambda - \Sigma\Delta T/2) \qquad (I-11)$$
$$J_+ = 2C\exp(-\Sigma^2\Delta T^2)erfc(\Lambda/2)$$
$$J_- = 2Cerfc(\Lambda)$$

where $\Lambda = 1/(4\Sigma\Delta T_{coin}), C$ is a constant that need not concern us. We remind the reader that the error function $erfc(x) \Rightarrow 0$ as $x \Rightarrow \infty$ and $erfc(x) \Rightarrow 2$ as $x \Rightarrow -\infty$. The key point to understand the behavior of the coincidence counting modulation is the variation of the J's with the increase of $\Delta T = \Delta L/c$.

(1). For $\Delta L < l_{coh}, J_0 = J_1 = 2J_+ = 2J_-$. From (I-10), the coincidence counting rate R_c has oscillations at ω_1, ω_2, and their sum and difference frequencies. The visibility is 100% in this case. As is seen in fig. I-2. As ΔL increases J_1 and J_+ rapidly decrease becoming negligible when ΔL is approaching l_{coh}, the coherence length of the down converted beam. This can be seen in fig. I-4, when $\Delta L = 115\mu m$ which is about one half of the coherence length l_{coh}, the beating component and the $632.8nm$ and $788.7nm$ components of the modulations are reduced and the sum-frequency modulation becomes predominant.

(2). $l_{coh} < \Delta L < c \cdot \Delta T_{coin}$, as ΔL increases to be greater than l_{coh} both J_1 and J_+ are zero and we left with

$$R_c = R_0[J_0 + J_-\cos(\Omega_p\Delta T)] \qquad (I-12)$$

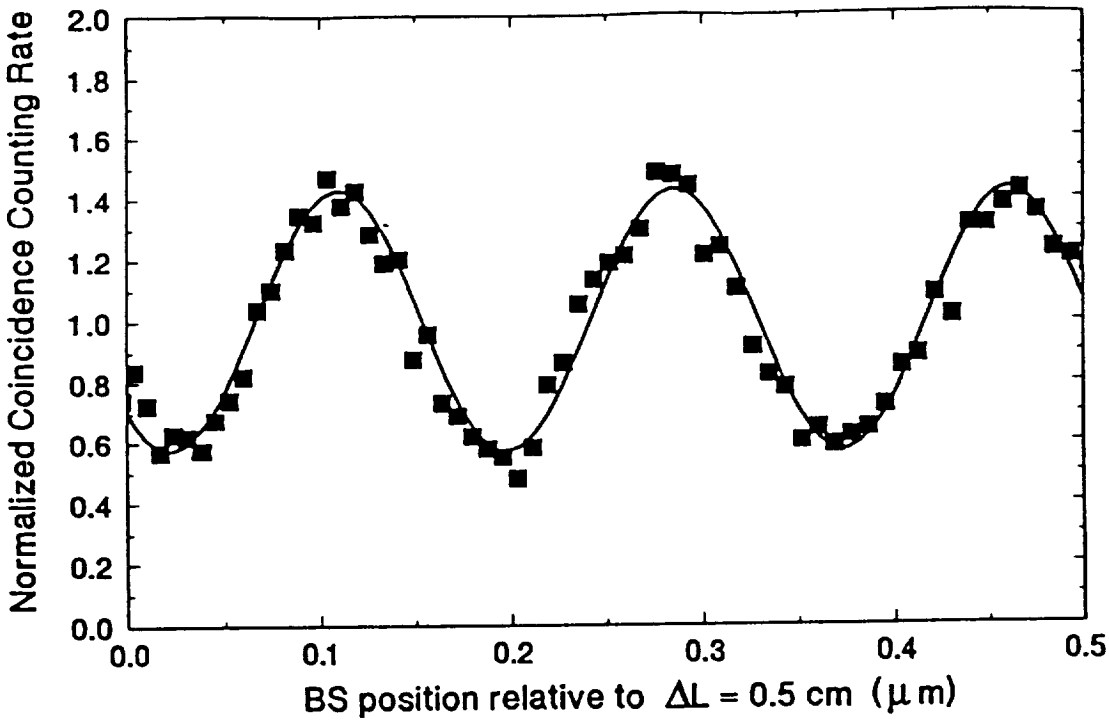

Figure I-6: Normalized coincidence counting rate of N_c at $\Delta L \cong 0.5\ cm$ for a $\Delta T_{coin} = 300psec$ time window. The beating modulation and the $\omega_1$and ω_2 modulations have completely disappeared. A visibility of $(44 \pm 3)\%$ was measured.

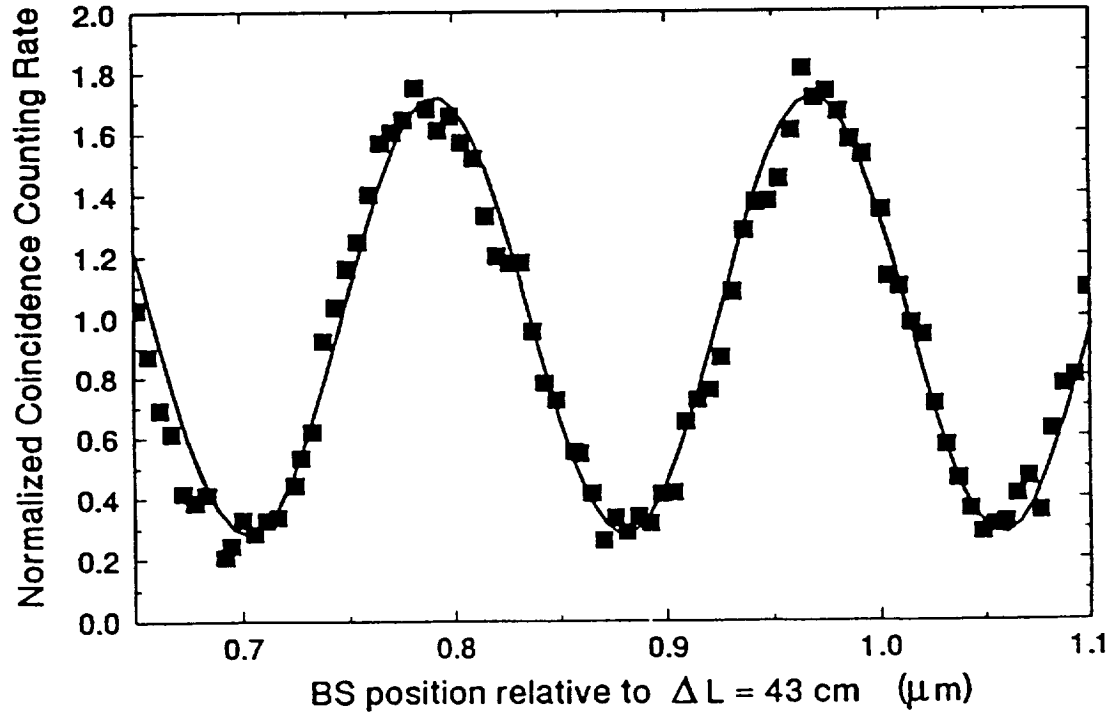

Figure I-7: Normalized coincidence counting rate of $N_c$at $\Delta L \cong 43cm$. The observed $(75 \pm 3)\%$ interference visibility marks the quantum interference effect. The modulation at $\lambda = 0.351\mu m$ is the sum frequency of the signal and idler light quanta.

which indicates that the modulation is only at the sum frequency. The modulation visibility can only approach to a maximum value of 50%, this is because the contribution of the last two terms in J_0 which arise from the state amplitudes in which one photon follow the longer and the other the shorter path of the interferometer. Fig. I-6 clearly shows this modulation.

(3). $\Delta L > c \cdot \Delta T_{coin}$. In this region, the interference pattern looks the same as in case (2). however, the interference visibility increases to more than 50%. This is because of the vanishing of the last two terms in J_0, the interference visibility is predicted to be 100% in idealized experimental conditions. This interference behavior is clearly demonstrated in fig. I-7.

The above simple theory of the quantum mechanical model provides a good quantitative understanding of what is happening in this experiment without the introduction of any artificial parameters. In the region of $\Delta L < l_{coh}$, all J's contribute to the interference pattern, which is not distinguishable from a classical model. In this region the first order interference pattern appears in both N_1 and N_2 counting. The coincidence modulation may explained as the result of the product of N_1 and N_2 modulations. When ΔL increases, J_1 and J_+ approach zero due to the vanishing of the factor $\exp(-\Sigma^2 \Delta T^2)$. This effect may be considered also to be a classical wave behavior. In the second region, $l_{coh} < \Delta L < c \cdot \Delta T_{coin}$, the coincidence interference behavior shown in (I-12) is expected. Since the ω_1 and ω_2 beams never meet at the same detector because of the filters, and each beam does not interfere with itself when $\Delta L > l_{coh}$, the coincidence modulation is a non-local two photon interference effect. In the third region, it is by now well known that under condition $\Delta L > c \cdot \Delta T_{coin}$, the interference is a purely quantum effect. It is impossible to have a classical model to explain the coincidence counting rate modulation of more than 50%. Mathematically the increase of the visibility is due to the vanishing of the factor $\exp(-\Delta T / 2\Delta T_{coin})$ in J_0. Physically this is due to the cut off by the coincidence time window of the state amplitudes in which one photon follows the longer path and other the shorter arm of the interferometer. This is equivalent to the projection of a quantum entangled EPR state [7, 8]

$$\Psi_{EPR} = A(t_1, t_2) + A(t_1 - \Delta T, t_2 - \Delta T) \qquad (I-13)$$

from the initial state. For $\Delta L > c \cdot \Delta T_{coin}$, the entangled two-photon EPR state (I-13) is realized by the measurement, which takes advantage of the particle nature of the light quanta in a wave-like experiment.

II Einstein-Podolsky-Rosen-Bohm Experiment By Splitting A Pair of Orthogonally Polarized Photon.

Type I parametric down conversion has drawn a great deal of attention since the first application [9] of it in an Einstein-Podolsky-Rosen-Bohm experiment [10]. The experimental study of Type II photon pairs was performed before Type I in our laboratory. However, the experimental results seemed to suggest that the orthogonally polarized signal and idler photon pair do not have the expected quantum entanglement. This phenomenon has troubled us and many other physicists with whom we have communicated in the past [11]. The entanglement of the Type II photon pair was demonstrated recently in our laboratory under two experimental conditions: (1) using a thin nonlinear crystal and (2) detecting coincidences in narrow spectral bandwidth [12, 13]. In

this section, we wish first to report the experimental study of this crystal length and detection bandwidth dependent entanglement of Type II down conversion. Then we report an experimental study of entangled two-photon EPR-Bohm states in Type II down conversion with linear, circular and elliptical polarizations.

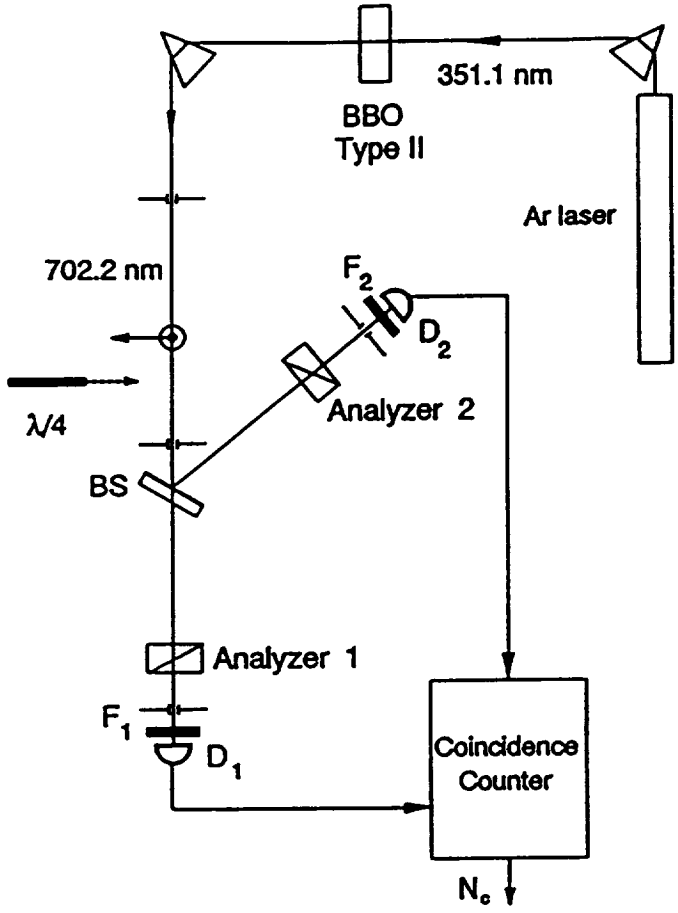

Figure II-1: Schematic experimental set up.

The experimental set up to study the effect of crystal length and detection bandwidth dependent entanglement is illustrated in fig. II-1. A single mode CW Argon ion laser line of $351.1nm$ was used to pump a BBO ($\beta - BaB_2O_4$) nonlinear crystal. The BBO was cut for a Type II phase matching condition to generate a pair of orthogonally polarized signal and idler photons collinearly and degenerately in $702.2nm$ wavelength. Two BBO crystals with lengths of $5.65mm$ and $0.5mm$, respectively, were used in the experiments. The $702.2nm$ pairs were separated from the pumping beam by a UV grade fused silica dispersion prism, then directed collinearly at a near normal incident angle to a polarization independent beam splitter which has $50\% - 50\%$ reflection and transmission coefficients. In each transmission and reflection output port of the beamsplitter a Glan Thompson linear polarization analyzer followed by a narrow bandwidth interference spectral filter were placed in front of a single photon detector. The photon detectors are dry ice cooled avalanche photodiodes operated in Geiger mode. The output pulses of the detectors were then sent

to a coincidence circuit with a $3nsec$ coincidence time window. The two detectors are separated by about $2m$, so that compared to the $3nsec$ coincidence window, the detections are space-like separated events. The coincidence counting rates were studied as functions of angles θ_1 and θ_2, where θ_i is the angle between the axis of the ith polarization analyzer and the direction, which is defined by the o-ray polarization plane of the BBO crystal. Keep in mind that a right-handed natural coordinate system with respect to the k_i vector as the positive direction is employed for the discussions in this paper. The following form of coincidence rate as a function of θ_1 and θ_2 was observed in the experiments,

$$R_c = R_{c0}(\cos^2\theta_1 \sin^2\theta_2 + \sin^2\theta_1 \cos^2\theta_2 - \rho \sin\theta_1 \cos\theta_2 \sin\theta_2 \cos\theta_1) \qquad (\text{II}-1)$$

where ρ is a parameter which depends on the crystal length, the detection bandwidth, and the group velocities of the $o-e$ beams inside the crystal. If $\rho = 2$, eq. (II-1) reduces to,

$$R_c = R_{c0} \sin^2(\theta_1 - \theta_2) \qquad (\text{II}-2)$$

which is the expected quantum correlation for the entangled two-photon EPR-Bohm state

$$|\Psi\rangle = 1/\sqrt{2}(|X_1\rangle \otimes |Y_2\rangle + |Y_1\rangle \otimes |X_2\rangle) \qquad (\text{II}-3)$$

$|\Psi\rangle$ quantum mechanically indicates a two-photon polarization state which is a superposition of the quantum probability amplitudes:

$$\begin{aligned} &(1)\ |o-ray\ transmitted\rangle \otimes |e-ray\ reflected\rangle \\ &(2)\ |e-ray\ transmitted\rangle \otimes |o-ray\ reflected\rangle \end{aligned} \qquad (\text{II}-4)$$

when the orthogonally polarized photon pair meets the beamsplitter. On the other hand, if $\rho = 0$ the interference cross term does not contribute. State (II-3) can not be concluded and no sign of the entanglement of the pair can be seen from the measurement.

Fig. II-2 reports the measured values of ρ for BBO crystals with lengths of $5.65mm$ and $0.5mm$ for different bandwidths of the filters. Note that for the $5.65mm$ BBO crystal ρ was always substantially less than 2 for the filters that used in the measurements. For the $0.5mm$ BBO, $\rho = 1.98$ was achieved with a $1nm$ bandwidth spectrum filter. The solid curves are the fits to a theoretical model which will be presented below. The values of ρ were obtained from the measurements of coincidence rate as functions of θ_1 and θ_2. Fig. II-3, fig. II-4 are typical measurements which reflect the different coincidence behavior for $5.65mm$ and $0.5mm$ BBO crystals. In fig. II-3, θ_1 was set to 45° and the coincidence rate was mapped out as a function of θ_2. In fig. II-4, both θ_1 and θ_2 were changed, keeping the sum of θ_1 and θ_2 equal to 90°. In both fig. II-3 and fig. II-4 the filters were $1nm$ bandwidth. By fitting many similar curves, $\rho = 0.72 \pm 0.07$ and $\rho = 1.98 \pm 0.04$ were determined for $5.65mm$ and $0.5mm$ crystals, respectively.

For Type II down conversion the two photon part of the state that exits the down conversion crystal may be calculated from the standard theory for parametric down conversion to be [6],

$$|\Psi\rangle = \iint d\omega_1 d\omega_2 \delta(\omega_1 + \omega_2 - \omega_p)\psi(\omega_1) a_o^\dagger(\omega_1(k_1)) a_e^\dagger(\omega_2(k_2)) \,|\, 0\rangle \qquad (\text{II}-5)$$

where ω and k represents the frequency and the wave vector for signal (1), idler (2), and pump (p). The frequency phase matching condition is explicitly displayed by the delta function, and the

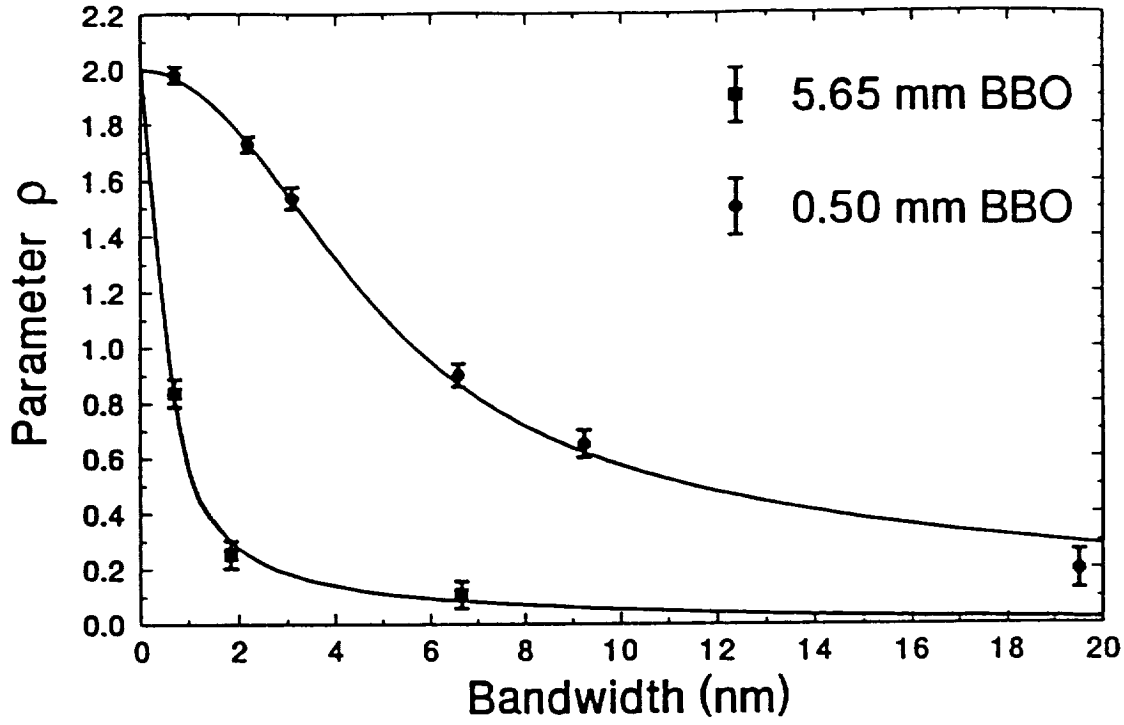

Figure II-2: Crystal Length and Detection Bandwidth Dependent Entanglement. The solid curve is a fitting of the theoretical mode.

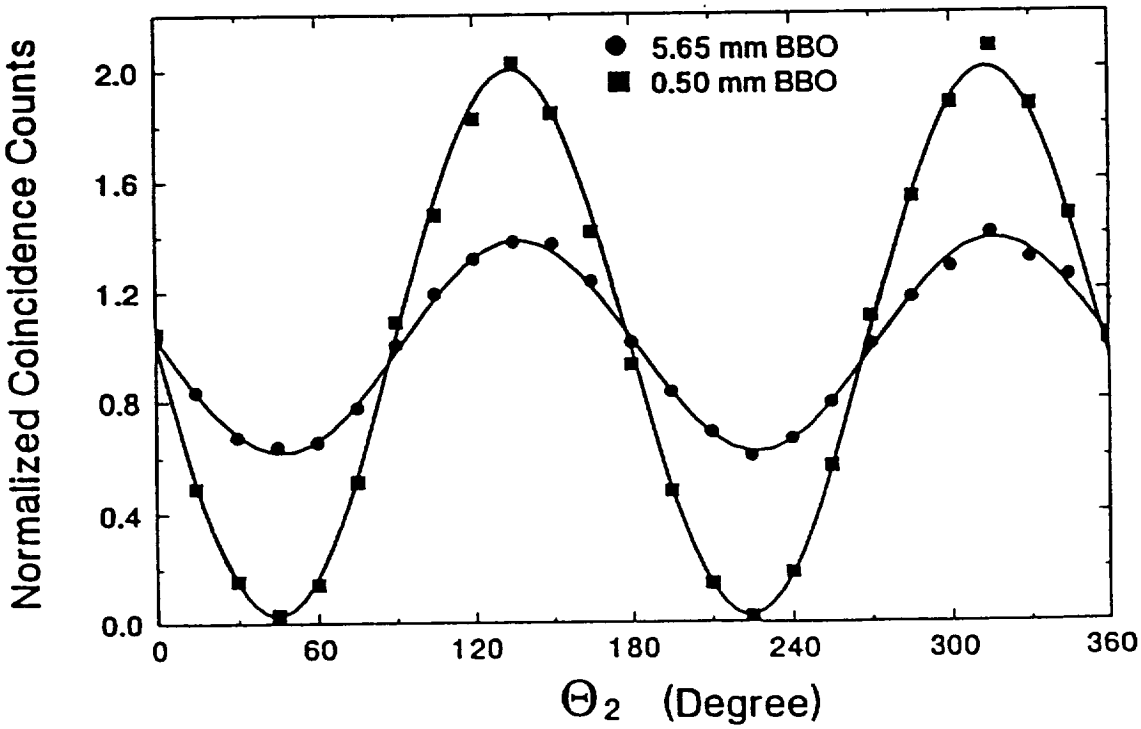

Figure II-3: Coincidence Measurements for Linear Polarization States when θ_1 was set equal to 45°.

wave number phase matching condition is implicit in the choice of the location of the detectors, in this experiment we consider collinear down conversion. The function $\psi(\omega)$ is determined from the standard theory of down conversion. It depends on the length of the crystal, and $D = c/u_o - c/u_e$. We shall refer to D as the two-photon dispersion. The subscript indies o and e for the creation operators indicate the ordinary and extraordinary rays of the down conversion, traveling along the same direction as the pump, the z-direction. The coordinate axes x and y are chosen along the the polarization direction of the o-ray and the e-ray, respectively.

The fields at the detectors 1 and 2 are given by

$$E_1^{(+)}(t) = \alpha_t \int d\omega f_1(\omega) \exp[-i\omega(t-\tau_1)] \sum_j \hat{e}_1 \hat{e}_j a_j(\omega)$$
$$E_2^{(+)}(t) = \alpha_r \int d\omega f_2(\omega) \exp[-i\omega(t-\tau_2)] \sum_j \hat{e}_2 \hat{e}_j a_j(\omega) \qquad (\text{II}-6)$$

where a_j is the destruction operator of the photons, $j = o, e$, i is in the direction of the ith linear polarization analyzer axis, $i = 1, 2$, α_t and α_r are the complex transmission and reflection coefficients of the beamsplitter. The function $f_i(\omega)$, $i = 1, 2$, is the spectral transmission coefficient function of the filter in front of the ith detector.

The counting rate can be written in terms of the square of the effective two-photon wave function (I-3), which has been used in the calculation of the first experiment. It is straight forward to show from (II-5),(II-6),

$$\Psi(t_1, t_2) = \alpha_t \alpha_r [\hat{e}_1 \cdot \hat{e}_o \; \hat{e}_2 \cdot \hat{e}_e A(t_1 - \tau_1, t_2 - \tau_2) + \hat{e}_1 \cdot \hat{e}_e \; \hat{e}_2 \cdot \hat{e}_o A(t_2 - \tau_2, t_1 - \tau_1)] \qquad (\text{II}-7)$$

where

$$A(t_1, t_2) = u(t_1 - t_2) \exp(-i\Omega_1 t_1) \exp(-i\Omega_2 t_2)$$
$$u(t) = A_0 \int d\omega f'(\omega) \psi'(\omega) \exp(i\omega t) \qquad (\text{II}-8)$$

where we have assumed that the filter f_1 and f_2 are peaked around Ω_1 and Ω_2, respectively, where $\Omega_1 + \Omega_2 = \omega_p$. For simplicity we take them to have the same shape so that $f'(\omega) = f_1(\omega + \Omega_1) = f_2(\omega + \Omega_2)$. ψ can be computed from the standard theory of optical parametric down conversion. Taking the origin of the coordinates at the output side of the crystal, and letting $\psi'(\omega) = \psi(\omega + \Omega_1)$, we find

$$\psi'(\omega) = [1 - \exp(-i\omega DL)]/i\omega D \qquad (\text{II}-9)$$

The average coincidence counting rate is given by (I-2). In the following calculation we assume $S(t, \Delta T_{coin}) = 1$ for a $3nsec$ time window ($t_1 - t_2 << \Delta T_{coin}$). Taking the filters to be Gaussian

$$f'(\omega) = f_0 \exp(-\omega^2/2\sigma^2) \qquad (\text{II}-10)$$

it is not difficult to show that the coincidence counting rate becomes

$$R_c = R_{c0}[\cos^2\theta_1 \sin^2\theta_2 + \sin^2\theta_1 \cos^2\theta_2 - \rho \sin\theta_1 \cos\theta_1 \sin\theta_2 \cos\theta_2] \qquad (\text{II}-11)$$

where

$$\rho = 2(C_+ - C_-)/(C_+ + C_-) \qquad (II-12)$$

with

$$C_+ = K \int_{-\infty}^{+\infty} dt[erfc(s+t) + erfc(s-t)]^2$$
$$C_- = K \int_{-\infty}^{+\infty} dt[2erfc(t) - erfc(s+t) + erfc(t-s)]^2 \qquad (II-13)$$

where erfc is the error function, K is a constant, and parameter

$$s = \sigma DL \qquad (II-14)$$

The only parameter that ρ depends is s, which shows the dependence on σ, the bandwidth of the filters, D, the two-photon dispersion, and L, the length of the crystal. By sketching the integrals, it is not difficult to show that for a very long crystal $\rho \cong 0$, because $C_+ - C \cong 0$, and for a short crystal $\rho \cong 2$, because $C \cong 0$.

The functions in (II-13) are easily evaluated numerically and fit the data accurately with no free parameters. The solid lines in fig. II-2 are the theory curves for $5.65mm$ and $0.5mm$ BBO crystals. The curves agree with the measured values of ρ within reasonable experimental error. One can achieve $\rho \cong 2$ with bandwidth filters less than $1nm$ for a $0.5mm$ BBO thin crystal.

Using a $0.5mm$ crystal and a $1nm$ bandwidth filter to achieve $\rho = 2$, measurements for two-photon polarization entangled EPR states were made. The use of a quarter wave plate and a beamsplitter easily can demonstrate the quantum mechanical entanglement of arbitrary elliptical polarization states in Type II down conversion. The experimental set up is the same as in fig. II-1, except a quarter wave plate is placed after the $0.5mm$ BBO crystal. If the fast axis of the quarter wave plate is oriented at angle Φ with respect to the direction, the orthogonal linear polarization states $\mid X\rangle$ and $\mid Y\rangle$ are transformed to orthogonal elliptical polarization states. After the beamsplitter a two-photon entangled state with elliptical polarizations is produced,

$$\mid \Psi\rangle = 1/\sqrt{2}\left[\begin{pmatrix} \cos\Phi \\ -i\sin\Phi \end{pmatrix}_1 \begin{pmatrix} \sin\Phi \\ -i\cos\Phi \end{pmatrix}_2 + \begin{pmatrix} \sin\Phi \\ i\cos\Phi \end{pmatrix}_1 \begin{pmatrix} \cos\Phi \\ i\sin\Phi \end{pmatrix}_2\right] \qquad (II-15)$$

where state $|\Psi\rangle$ is a superposition of the quantum probability amplitudes:

(1). $(\cos\Phi \mid X'\rangle - i\sin\Phi \mid Y'\rangle)transmitted \otimes (\sin\Phi \mid X'\rangle + icos\Phi \mid Y'\rangle)reflected$

(2). $(\sin\Phi \mid X'\rangle + i\cos\Phi \mid Y'\rangle)transmitted \otimes (\cos\Phi \mid X'\rangle - i\sin\Phi \mid Y'\rangle)reflected$

when the orthogonal elliptical polarized photon pair meets the beamsplitter.

The coincidence counting rate for linear polarization analyzers is then,

$$R_c = R_{co}[\sin^2(2\Phi)\cos^2(\theta_1' + \theta_2') + \cos^2(2\Phi)\sin^2(\theta_1' - \theta_2')] \qquad (II-16)$$

where θ_i' is the angle between the axis of the ith polarization analyzer and the $|X_i'\rangle$ direction. Care has to be taken to follow the rules of natural coordinate system, especially for the reflected beam. Note that the direction of $|X_2'\rangle$ is opposite to that of $|X_1'\rangle$.

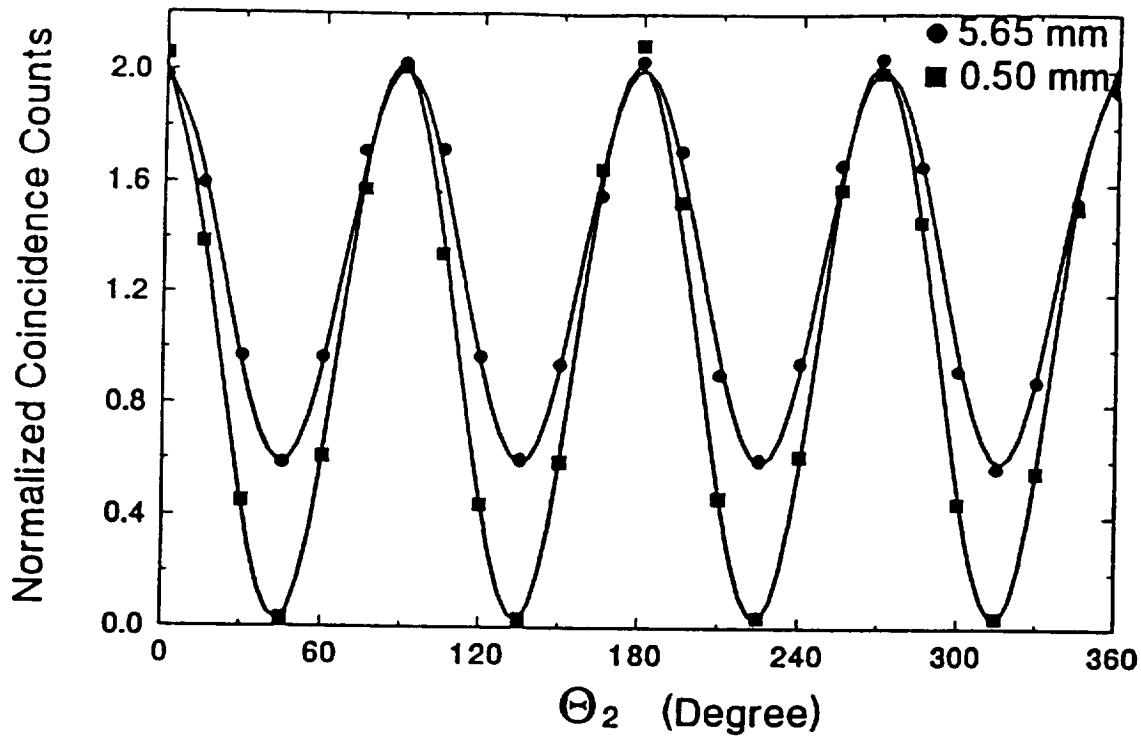

Figure II-4: Coincidence Measurements for Linear Polarization States when $\theta_1 + \theta_2 = 90°$was preserved.

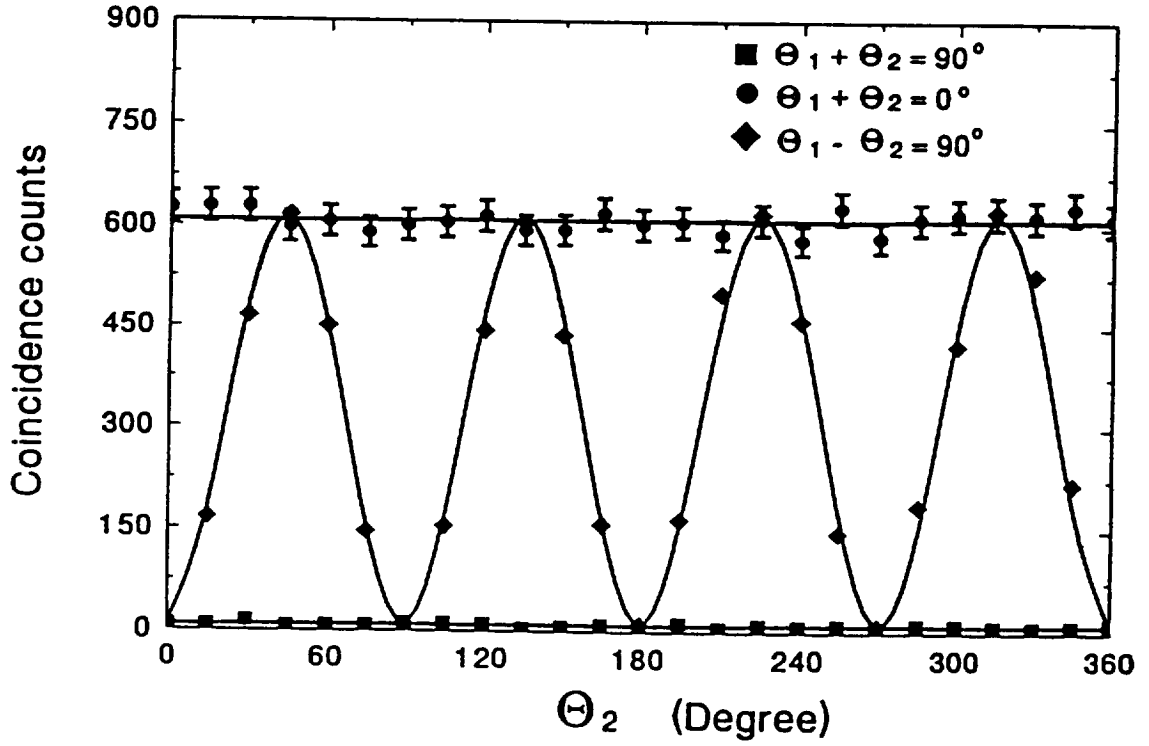

Figure II-5: Coincidence Measurements for Circular Polarization EPR-Bohm State.

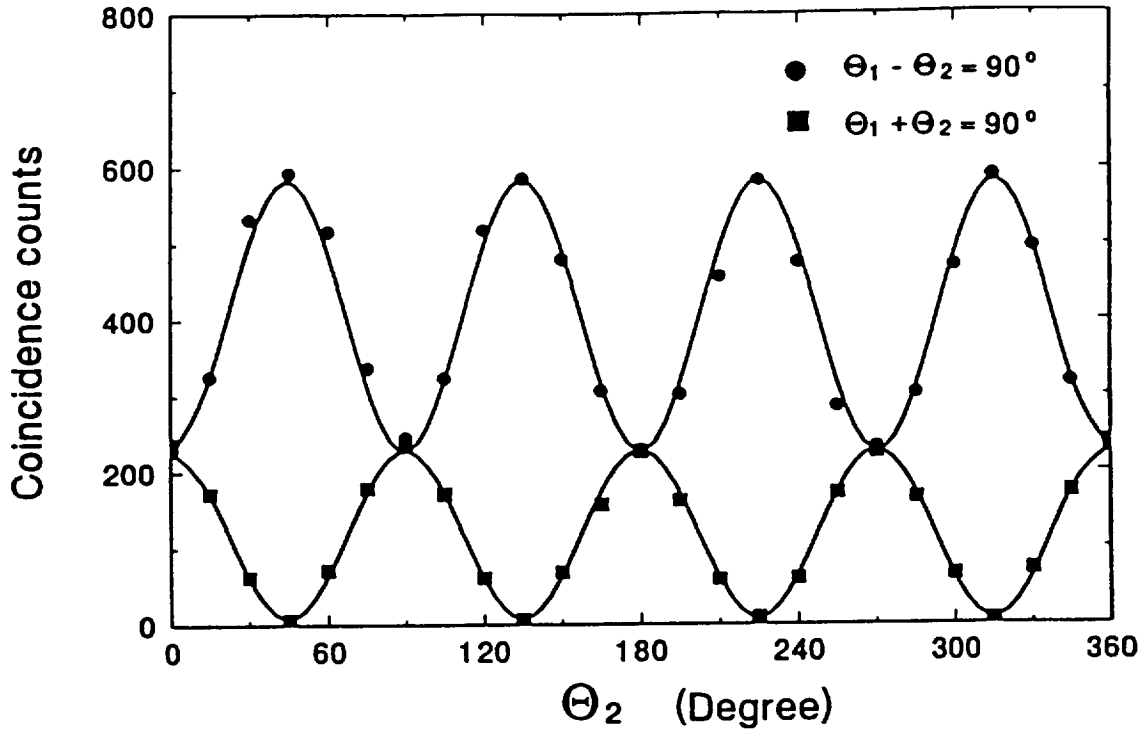

Figure II-6: Coincidence Measurements for Elliptical Polarization State with Quarter Wave-plate oriented at 26.5°.

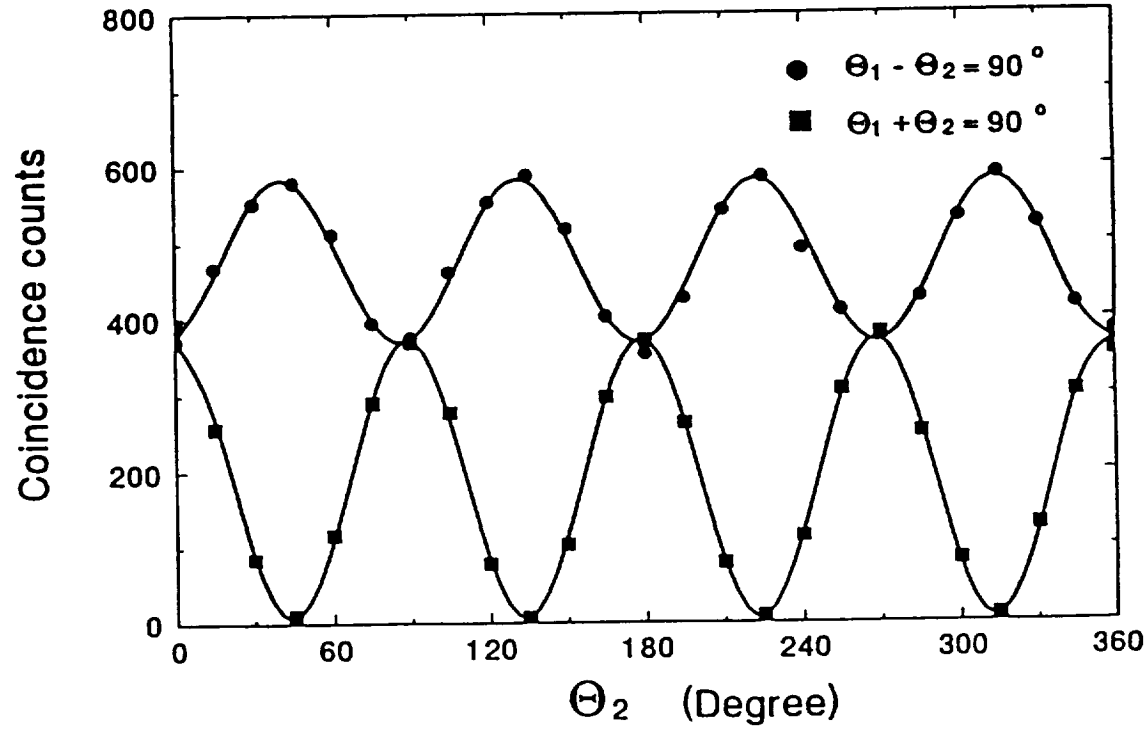

Figure II-7: Coincidence Measurement for Elliptical Polarization State with Quarter Waveplate oriented at 71.5°.

If $\Phi = 0°$, state (II-15) becomes state (II-3) which is a two-photon linear polarization entangled state. Quantum correlations given by eq. (II-2) were observed experimentally, see fig. II-3 and fig. II-4, with modulations about$(98 \pm 2)\%$.

For $\Phi = 45°$. State (II-15) becomes the circular polarization EPR-Bohm state,

$$| \Psi) = 1/\sqrt{2}(| R_1\rangle \otimes | R_2\rangle + | L_1\rangle \otimes | L_2\rangle) \qquad (\text{II}-17)$$

The expected quantum correlations

$$R_c = R_{c0} \cos^2(\theta_1 + \theta_2) = R_{c0} \cos^2(\theta_1' + \theta_2') \qquad (\text{II}-18)$$

were measured experimentally. Fig. II-5 reports the measured results. The modulation is about $(98 \pm 2)\%$.

When the quarter wave plate was set to $\Phi = 26.5°$ and $71.5°$, fig. II-6 and fig. II-7 report four typical measurements which were taken under the conditions: $\theta_1' \pm \theta_2' = 90°$. The solid lines in these figures are the theory curves of (II-18). Note, here, we use θ' system to define the angles for the analyzers.

Contrary to the coincidence counting rate, the single detector counting rate remains constant for all the above measurement. Fig. II-8 reports a typical counting rate for detector 2 in a measurement.

A pair of orthogonally polarized light quanta enters a single port of a beamsplitter, if one of the photons, for example the transmitted one, is detected to be linearly polarized in a certain direction, θ_1, the other one can be predicted with certainty to be linearly polarized in the direction θ_2. This makes the experiment EPR type argument. Addition to this argument, it is also interesting to see that θ_2 is not necessarily perpendicular to θ_1, the value of θ_2 depends on the EPR state prepared by the observer.

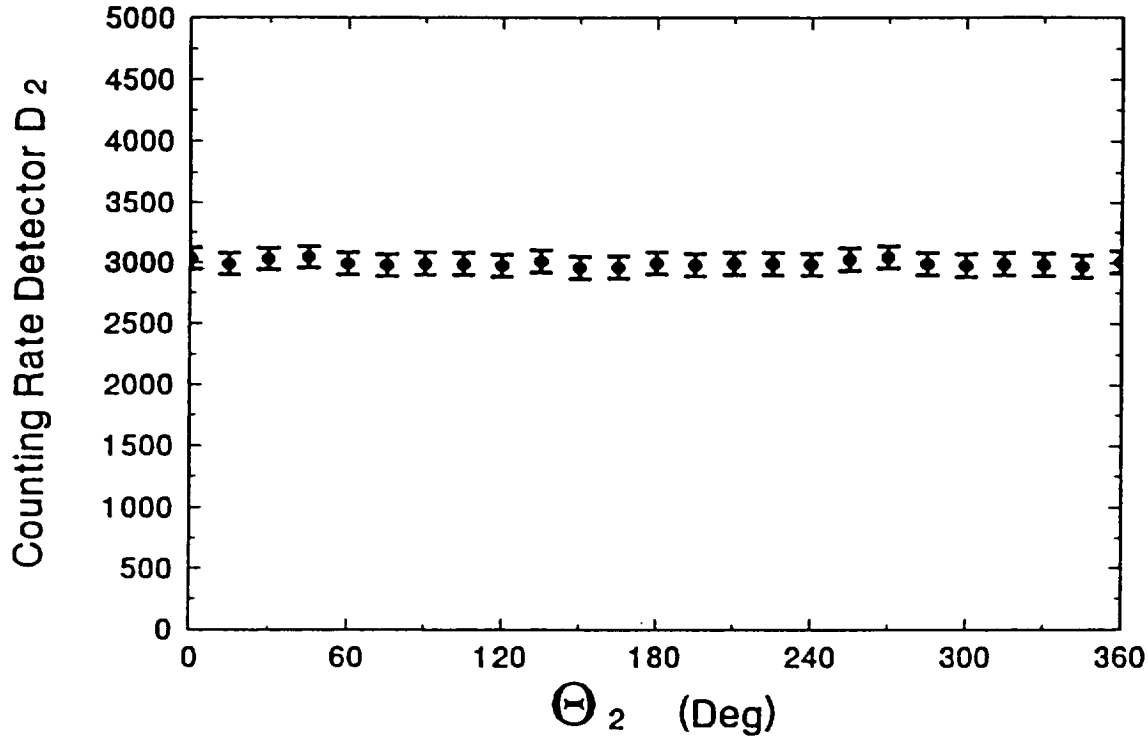

Figure II-8: Single detector counting rate.

This simple beam-splitting experiment is a particle-like experiment. Eq. (II-4) is based on the argument that the photon can be either transmitted or reflected by a beamsplitter. On the other hand this simple beam-splitting type experiment demonstrated the wave property of the photon. The 100% modulation of the coincidence counting rate is essentially an interference superposition of the two-photon amplitudes in (II-7). The overlap and non-overlap of the amplitudes $A(t_1 - \tau_1, t_2 - \tau_2)$ and $A(t_2 - \tau_2, t_1 - \tau_1)$ is a good measure of the wave packet picture of the photon, which results the crystal length and detection bandwidth dependent of the two-photon entanglement.

We wish to thank D.N. Klyshko for many useful discussions. This work was supported partially by the Office of Naval Research Grant No. $N00014 - 91 - J - 1430$.

References

[1] A. Einstein, B. Podolsky and N. Rosen, Phys. Rev. 47, 777 (1935).

[2] M.H. Rubin and Y.H. Shih, Phys. Rev. A 45, 8138 (1992).

[3] J.D. Franson, Phys. Rev. Lett. 62, 2205 (1989).

[4] Y.H. Shih, A.V. Sergienko, and M.H. Rubin, Phys. Rev. A 47, 1288 (1993).

[5] P.G.Kwiat, A.M. Steinberg, and R.Y. Chiao, Phys. Rev. A 47, 2472 (1993).

[6] D.N. Klyshko, Photons and Nonlinear Optics, Gorden and Breach Science Publishers, N.Y., (1988).

[7] E.Schrödinger, Naturwissenschaften, 23, 807, 823, 844 (1935). A translation of these papers appears in J.A. Wheeler and W.H. Zurek, ed., Quantum Theory and Measurement, Princeton University Press, (1983).

[8] M.A. Horne, A. Shimony, and A. Zeilinger, Phys. Rev. Lett. 62, 2209 (1989).

[9] C.O. Alley and Y.H. Shih, Foundations of Quantum Mechanics in the Light of New Technology, ed. M.Namiki et. al., p. 47 (1986). Y.H. Shih and C.O. Alley, Phys. Rev. Lett. 61, 2921 (1988).

[10] D. Bohm, Quantum Theory, Prentice Hall, Englewood Cliffs, (1951).

[11] Private communications with J.A. Wheeler, E.P. Wigner, A. Shimony, J.D. Franson and others.

[12] T.E. Kiess, Y.H. Shih, A.V. Sergienko, and C.O. Alley, Phys. Rev. Lett., **71**, 3893 (1993).

[13] Y.H. Shih, A.V. Sergienko, M.H. Rubin, T.E. Kiess and C.O. Alley, Submitted to Phys. Rev. A, (1993).